Wireless Environmental Sensor Networking With Analog Scatter Radio and Timer Principles

Eleftherios Kampianakis, *Student Member, IEEE*, John Kimionis, *Student Member, IEEE*, Konstantinos Tountas, Christos Konstantopoulos, Eftichios Koutroulis, *Member, IEEE*, and Aggelos Bletsas, *Senior Member, IEEE*

Abstract—**Environmental variables monitoring with wireless sensor networks (WSNs) is invaluable for precision agriculture applications. However, the effectiveness of existing low-power, conventional (e.g., ZigBee-type) radios in large-scale deployments is limited by power consumption, cost, and complexity constraints, while the existing WSN solutions employing nonconventional, scatter-radio principles have been restricted to communication ranges of up to a few meters. In this paper, the development of a novel analog scatter-radio WSN is presented, that employs semipassive sensor/tags in bistatic topology (i.e., carrier emitter placed in a different location from the reader), consuming <1 mW of power, with communication range exceeding 100 m. The experimental results indicate that the multipoint surface fitting calibration, in conjunction with the employed two-phase filtering process, both provide a mean absolute error of 1.9% environmental relative humidity for a temperature range of 10 °C–50 °C. In addition, the energy consumption per measurement of the proposed environmental monitoring approach can be lower than that of conventional radio WSNs. Finally, the proposed approach operational characteristics are presented through a real-world network deployment in a tomato greenhouse.**

Index Terms—**Scatter radio communication, precision agriculture, backscatter sensor networks, environmental monitoring.**

I. INTRODUCTION

WIRELESS sensor networks (WSNs) have attracted great academic and industrial attention, with various applications ranging from environmental sensing and wearable biometric monitoring to security and structural monitoring [1]–[5], that perhaps realize the "Internet of Things" concept. Despite the fact that a lot of algorithm- and networking-related research has been conducted regarding
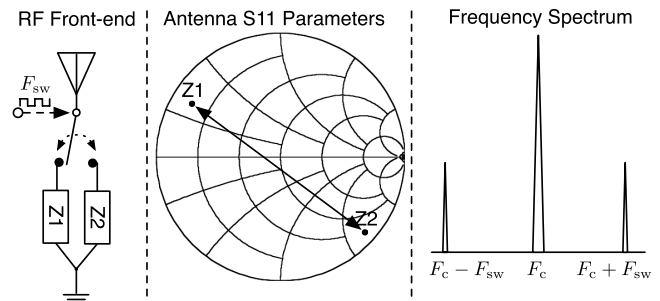
Fig. 1. Backscatter communication principle: RF switch alternates the loads of the tag antenna with frequency F_{sw}. When a carrier is imminent with frequency F_c, two subcarriers appear, with frequencies $F_c \pm F_{sw}$.

large-scale WSNs (e.g. work in [6]–[10]), only few examples of real-world large-scale deployments exist in the literature. For example, work in [11] demonstrated a network of a few hundreds of nodes and described the scale-vs-lifetime tradeoff. In that work, the cost of each sensor was approximately 36 €. Apart from the lifetime and cost constraints, software complexity has also been indicated as a major limiting factor for WSN scalability [12].

In order to address these constraints and promote network scalability, systems have emerged that utilize communication by means of reflected (and scattered back) radio frequency (RF) power; such concept has its roots back in the 1948 [13]. The most popular system of this technology is the radio frequency identification (RFID) tag, which is commercially utilized as a barcode-replacement for identification of objects or individuals.

In principle, backscatter communication is implemented with an RF switch (e.g. a single transistor) that alternates the termination load of an antenna between two (or more [14]) loads. As depicted in Fig. 1, if the antenna load termination is alternated with frequency F_{sw} while a continuous wave (CW) with frequency F_c is incident on the antenna (and produced by a distant emitter), then two subcarriers will emerge in the frequency spectrum, at frequencies $F_c \pm F_{sw}$. The RF front-end of such backscatter-enabled tag, can be implemented with minimal number of simple electronic circuit components, greatly reducing cost and complexity per tag, and thus, enabling large-scale deployments. The design of a frequency-modulated passive wireless sensor tag for ammonia sensing has been presented in [15], but its operation within a WSN structure has not been explored.
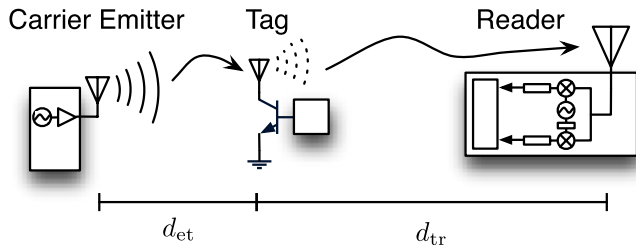
Fig. 2. Bistatic scatter-radio topology; carrier emitter placed in a different location from the reader. d_{et} and d_{tr} denote the emitter-to-tag and tag-to-reader distance, respectively.

Classic battery-less RFID systems utilize monostatic architectures (i.e. reader in the same box as the carrier emitter) and incorporate high bitrate schemes that greatly reduce the communication range down to a few meters [16]. On the other hand, environmental monitoring WSNs do not require either battery-less setups or high bitrates, since environmental variables, such as relative humidity (%RH) and temperature, change with a slow rate. With the utilization of the bistatic topology, illustrated in Fig. 2, where the carrier emitter is placed in a different location from the reader, the roundtrip path losses can be reduced, especially when more than one low-cost emitters illuminate the population of the tags (and thus, the probability of a short distance between emitter and tag is relatively high, for given tag-to-reader distance) [17]. Additionally, employing low bitrate increases the sensitivity of the receiver (reader) [18]. Finally, in order to avoid powering issues at the tag, each sensor/tag can be equipped with batteries (or other independent energy source e.g. a solar panel) [18]; in that way, more energy from the incoming wave can be reflected towards the reader, instead of using a fraction of the incoming energy to power the tag/sensor's electronics. The aforementioned techniques are utilized in [19], where tag-to-reader (d_{tr}) and emitter-to-tag (d_{et}) distances of over 134 m and 4 m, respectively, were demonstrated, with bit-error-rate (BER) on the order of 2%, frequency-shift keying (FSK) modulation, emitter power at 13 dBm, commodity software-defined receiver and carefully-designed non-coherent detection algorithms. Other examples in the literature that demonstrate the potential of backscatter radio for wireless sensor networking can be found in [20] and [21]. Moreover, a recent example of real-world deployment includes [22], in which the authors developed a scatter-radio sensor network that monitors ambient relative humidity (%RH), while an experimentation testbed for developing and optimizing backscatter-based WSNs was presented in [23].

Relative humidity (%RH) is an environmental variable that greatly affects growth of plants. Thus, it is particularly useful to monitor %RH variation across extended areas in either outdoor fields or greenhouses. Increased values of %RH can promote the growth of various bacteria such as Botrytis [24], or decrease the plant's mineral intake [25]. There are numerous implementations of low-power %RH sensors in the literature, (see [26], [27]), which however do not employ any wireless interface for transmitting information. On the other hand, passive wireless sensors have been used in [28] and [29] for

data transmission. However, these utilize inductive coupling techniques, which inherently limit the communication range to a few centimeters. Finally, classic WSNs for environmental monitoring have been presented in the literature [30]–[32], employing active IEEE 802.15.4 / ZigBee compliant, conventional RF transceivers, but their operation is limited due to power, complexity and cost constraints, discussed above.

In this paper, the design of an analog scatter-radio WSN is presented, which facilitates large-scale deployment of low-cost and low-power relative humidity sensors. In contrast to existing scatter-radio sensors with short communication range, this work utilizes bistatic topology and semi-passive (i.e. energy-assisted) tags that offer ranges on the order of 130 meters. The contribution of this work is summarized as follows:

- Design and fabrication of prototype %RH sensing tags, with *off-the-shelf* components, that exploit analog frequency modulation (FM), scatter-radio and sensor networking principles.
- Calibration and accuracy-characterization procedure of the developed sensor tags by taking into account not only humidity, but also temperature for the calculation of the sensor's characteristic function.
- Receiver design and implementation with a commodity software-defined radio (SDR) platform for the demodulation of the FM signals, backscattered by the tags.
- Data smoothing, exploiting a two-phase filtering process that actively increases the signal-to-noise ratio (SNR) at the reader and thus, offers longer communication ranges.
- Range characterization of point-to-point links through outdoor experimentation.
- Real-world deployment of a 10-sensor WSN for monitoring %RH, in a tomato greenhouse at the Mediterranean Agronomic Institute of Chania, Crete (MAICh).

This paper is organized as follows: the development of the analog wireless sensor is described in Section II, design and operation of the software-defined receiver are analyzed in Section III and experimental results are presented in Section IV. Work is concluded in Section V.

II. ANALOG WIRELESS SENSOR DESIGN

A. Description

The proposed WSN consists of low-power and low-complexity analog wireless sensors, which operate with scatter-radio principles. The circuit diagram and the prototype sensor/tag[1] which was developed, are depicted in Figs. 3 and 4, respectively. The sensor driving circuit is a capacitance-to-frequency converter with its output connected to a radio frequency (RF) switch; the latter consists of a single transistor. For the capacitance-to-frequency conversion, the Intersil 7555 timer IC is utilized and it has been configured to operate in astable multivibrator mode. The timer IC is connected to a resistor-capacitor (RC) network that contains the Honeywell HCH1000 capacitive relative humidity (%RH) sensor (i.e. C_{RH} in Fig. 3).

---

[1] In line with standard RFID terminology, the terms "tag" and "sensor" will be used interchangeably.
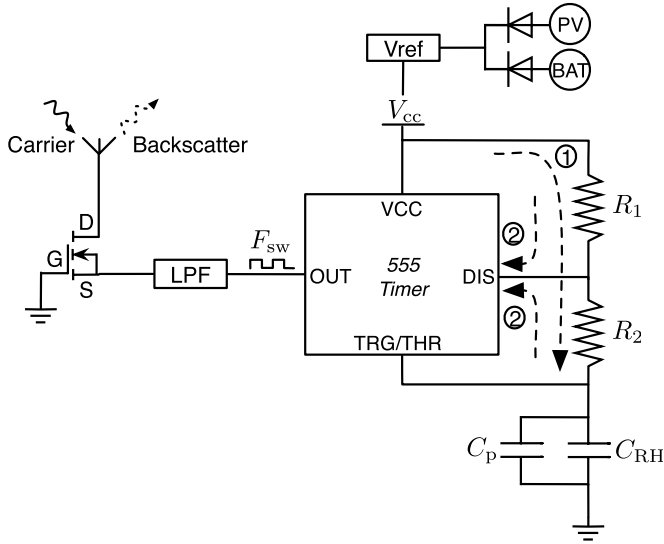
Fig. 3. Sensor circuit diagram with scatter-radio: capacitance varies the timer output frequency, producing a variable-frequency pulse that switches a single transistor; the latter is directly connected to the antenna.
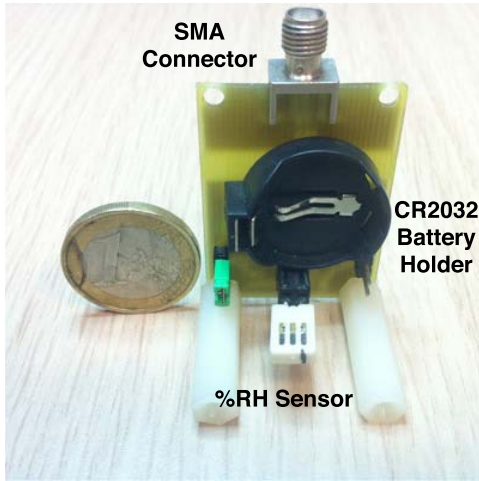

Fig. 4. The prototype sensor tag developed.

The RH sensing capacitor is periodically charged and discharged through resistors R_1 and R_2 (Fig. 3). Thus the frequency F and duty cycle D of the square wave produced at the output of the astable multivibrator are given by:

$$F = \frac{1}{(R_1 + 2R_2)C \ln(2)}, \tag{1}$$

$$D = \frac{R_1 + R_2}{R_1 + 2R_2}. \tag{2}$$

It is noted that D is always over 50 % since $R1 > 0$. Therefore, the proposed design produces a scatter-radio subcarrier (i.e. switching) frequency, which is dependent on the relative humidity value when a CW is incident on the antenna. In order to adjust the total capacitance range of the sensor tag, capacitor C_p is connected in parallel with the sensing capacitor. Thus, the total capacitance C is given by:
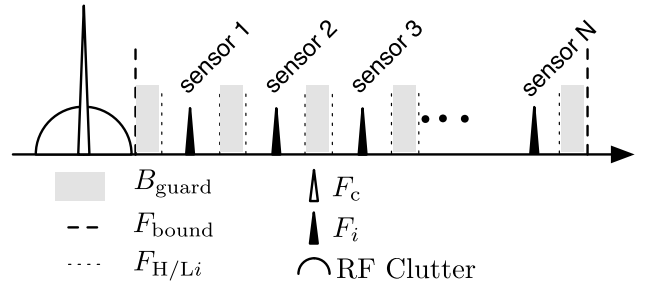
$$C = C_p + C_{RH}. \tag{3}$$

Fig. 5. Scheme for networking multiple tags. Each tag operates in different frequency bands, while guard bands are set up in between to avoid collision.

The RF front-end of the sensor tag consists of a single depletion-type MOSFET transistor, a low-pass filter and an antenna (implementation details in [33]). The NXP BF1118 transistor with a $V_p = -2$ V pinch-off voltage is used due to its low-cost, low gate-to-source leakage current (100 nA), high off-state isolation (30 dB) and low on-state insertion loss (below 2.5 dB). In order to turn the transistor "off", its gate is permanently connected to the ground and the voltage pulses from the timer, drive the MOSFET source. Therefore, when timer OUT pin is "high", the MOSFET gate-source voltage is set at $V_{gs} = -2$ V and the transistor is turned "off", else it is turned "on". Moreover, for decoupling the RF front-end from the timer circuit, an inductive filter bead has been utilized.

The components used to construct the prototype sensor/tag were selected such that a balance between cost, power consumption and performance is preserved. Using *off-the-shelf* electronic components, resulted in the relatively low cost in terms of bill of materials (BOM) of 5 € per tag, without including the SMA antenna connector, since the antenna can be easily integrated within the tag circuitry.

The wireless sensor design described above can be easily adapted for hosting alternative types of capacitive or resistive sensors for measuring environmental variables of interest (e.g. ambient temperature, water soil content, soil temperature etc.).

B. Multiple Access From Receiver-Less Sensors

In order for multiple tags to be able to communicate with the receiver, a medium access control (MAC) scheme was implemented. As noted above, each tag produces a subcarrier with an operating frequency that is related to the %RH value. In order for multiple *receiver-less* tags to be able to communicate *simultaneously* with the receiver, each tag of the network operates in a different frequency band [18], [34]. The concept is depicted in Fig. 5, where a specific frequency band is allocated for each tag, while guard-bands are also employed between adjacent bands in order to avoid collisions. This scheme, namely frequency division multiple access (FDMA), is also utilized in analog FM radio, where each radio channel accounts for a specific frequency [35].

The architecture of the proposed WSN is illustrated in Fig. 6. Low-cost emitters of the carrier CW are installed in a field and around them, multiple, scatter-sensors are spread. When the emitters are activated, cells are formed around
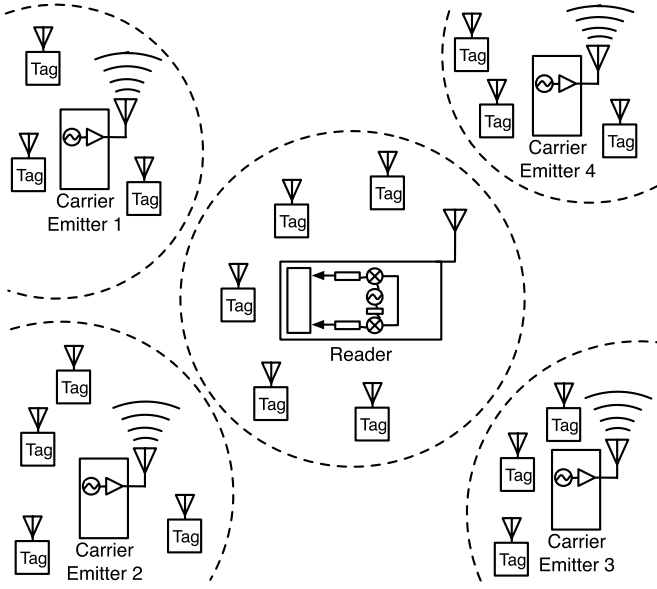
Fig. 6.   Proposed WSN overview. Multiple, low-cost carrier emitters are placed in the field and around them, many ultra low-power tags are deployed.

Fig. 8.   Temperature is included as a calibration parameter and thus the characteristic function is the surface RH(F,Temp).
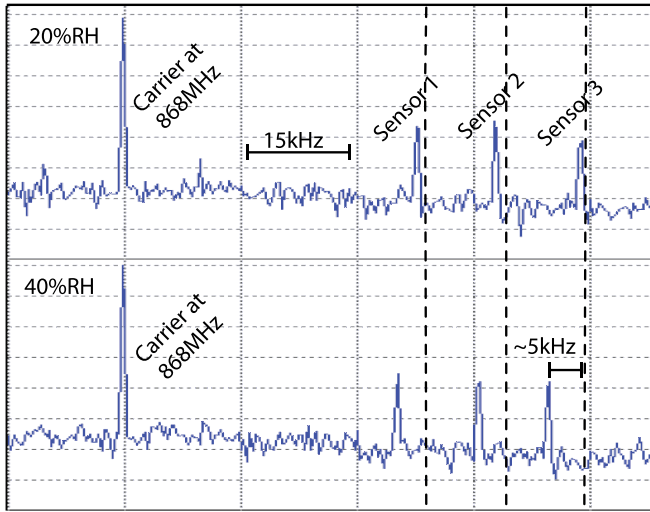

Fig. 7.   Experimental example: the subcarrier frequency shift of three sensors with change in %RH.

them containing groups of tags; each of these tags backscatters information to the receiver. The tags inside each cell employ the aforementioned FDMA scheme, whereas the carrier emitters operate based on a Time Division Multiple Access (TDMA) scheme. Specifically, the reader is responsible of switching on each carrier emitter separately, such that collisions are avoided. This way, the development of scatter sensor networks, consisting of hundreds of low-cost tags is feasible. As an example, the spectra of the backscattered signals from three sensors operating simultaneously are depicted in Fig. 7. Frequency shifting of the produced subcarriers is observed when relative humidity changes from 20 % to 40 %, while, simultaneously, signal collision is avoided.

The FDMA medium access scheme of the proposed WSN is implemented by selecting the appropriate component values
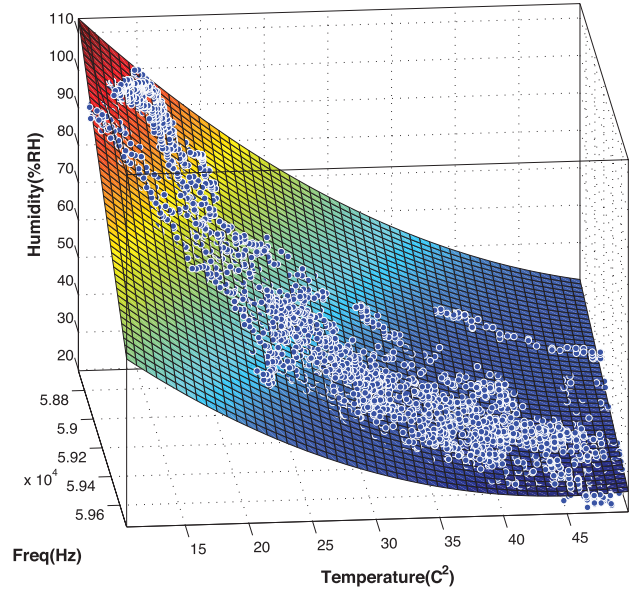
for the RC network of the timer in each individual tag, such that the center frequency and the total spectrum occupied by the corresponding tag are unique. Particularly, the spectrum band occupied by the i-th tag depends on the highest and lowest subcarrier frequency F_{Hi} and F_{Li}, respectively. Using (1), the total bandwidth B_i for the i-th tag is calculated according to the following equation:

$$
\begin{aligned}
B_i &= F_{Hi} - F_{Li} \\
&\overset{(1)(3)}{=} \frac{1}{R_i(C_L + C_{pi})\ln(2)} - \frac{1}{R_i(C_H + C_{pi})\ln(2)} \\
&= \frac{C_H - C_L}{\ln(2)R_i(C_L + C_{pi})(C_H + C_{pi})},
\end{aligned}
\tag{4}
$$

where $R_i = R_{1i} + 2R_{2i}$ and C_L and C_H are the sensing capacitance values for 0 %RH and 100 %RH, respectively. The values of R_i and C_{pi} are calculated using (1) and (4), as follows:

$$
C_{pi} = \frac{B_i C_L + F_{Li}(C_H - C_L)}{B_i},
\tag{5}
$$

$$
R_i = \frac{B_i}{\ln(2)F_{iL}(C_H - C_L)(F_{Li} + B_i)}.
\tag{6}
$$

Using the above methodology, the proposed implementation of collision-free access from multiple, receiver-less, analog sensors becomes straightforward.

C. Calibration and Accuracy

Target applications of the proposed WSN include environmental monitoring in outdoor deployments. It is important to note that the outdoor environment temperature variations significantly affect the operation of the electronic circuits within the sensor tag. As an example, the 7555 timer exhibits a temperature drift of 150 ppm/ °C and, thus, for a tag with nominal subcarrier frequency 50 kHz, a total change of 15 °C
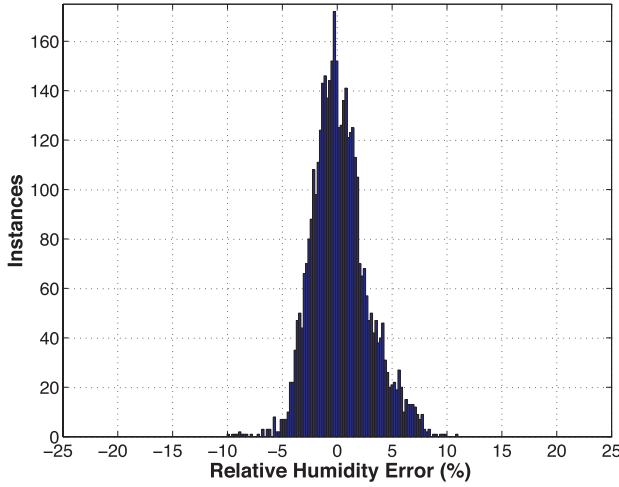
Fig. 9.   Measured %RH error histogram.

Fig. 10.   Reference versus received %RH measurements.

results to a frequency shift of 112.5 Hz. Considering that a typical tag occupies a bandwidth of 2 kHz, the aforementioned frequency shift amounts to 5.625 % of the tag's bandwidth and a %RH error of the same order (in percentage). In order to compensate for this effect, a calibration process is employed, considering both the ambient temperature and the sensor tag subcarrier frequency as input parameters.

Specifically, groups of five sensors were placed outdoors with their capacitive elements in adjacent positions. The Tinytag TGP-4500 from Gemini, which is a high-precision industrial humidity/temperature data-logger, was also placed in close proximity with the tags, for reference. The system was deployed to operate for 3 days and each sensor's subcarrier frequency was monitored at the reader, as analyzed next, while temperature and humidity from the reference sensor was logged every minute. A total of 4200 samples were collected and time-synchronized, using the timestamps from both the data-logger and the reader. Subsequently, polynomial surface fitting was applied in order to produce the calibration function, which is shown in Fig. 8. Due to the tolerance of the capacitance/resistance of commercial components, which affects the operating frequency of the timer, the calibration procedure described above should be applied for each sensor node before incorporation in the proposed WSN.

The measurement accuracy was characterized as follows: the collected subcarrier frequency and temperature data were utilized as inputs for the calibration function and the results were then compared to the reference measurements. The resulting relative humidity measurement error histogram and measured values are depicted in Figs. 9 and 10, respectively, operating a reference sensor and the calibrated tag in the 10-50 °C temperature range. The root mean squared error (RMSE) and the mean absolute error of the particular calibrated tag were 2.5 %RH and 1.9 %RH, respectively. Also, for 95 % of the samples, where humidity varied from 20 %RH to 100 %RH, the absolute error was less than 5 %RH. For the case of tag calibration under constant temperature of 25 °C, the corresponding accuracy was higher, exhibiting an RMSE of 0.86 %RH and a mean absolute error of 0.63 %RH.
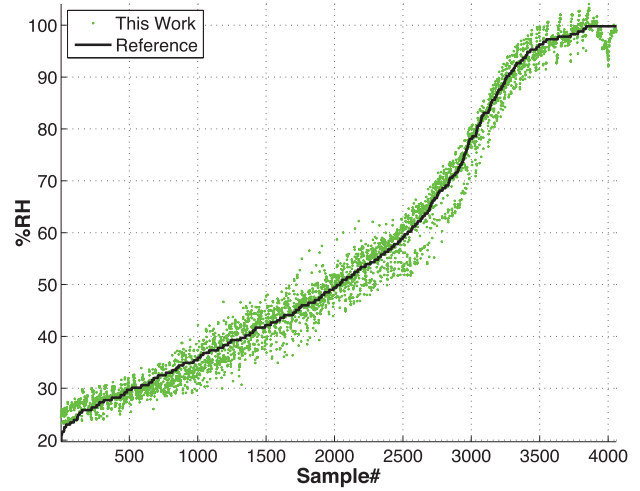
Similarly, for 95 % of the samples at 25 °C, the absolute error was less than 1.8 %RH.

D. Power Consumption and Tradeoff

As depicted in Fig. 3, each sensor is power-supplied through a voltage reference integrated circuit (IC) and two Schottky diodes, in common cathode configuration. Each of the diodes is connected to a different power source; a small solar panel with an open-circuit voltage of 3.5 V and a 3 V lithium-ion battery (type CR2032), respectively. The diodes act as a logic 'OR' and allow current to flow from the source with the largest voltage potential to the tag circuitry. Thus, the sensor power-supply alternates between battery and solar panel during night and day, respectively.

The tag operates from an input voltage of $V_{cc} = 2.26$ V and its total power consumption is given by:[2]

$$P_{tot} = P_{ch} + P_q + P_{R_1} + P_d, \qquad (7)$$

where P_{ch} is the average power required for charging the timer capacitors, P_q is the quiescent power dissipated by the timer and the voltage reference IC, P_{R_1} is the power dissipated on resistor R_1 and P_d is the power dissipated on the diodes. With the particular components utilized, $P_q = 220$ μW. Moreover, the value of P_d is equal to the forward voltage V_f of the diodes (for Schottky diodes, $V_f = 0.25$ V), multiplied by the current drawn by the tag:

$$P_d = \frac{V_f}{V_{cc}}(P_{ch} + P_q + P_{R_1}). \qquad (8)$$

During the 555 timer operation, the total capacitance $C = C_p + C_{RH}$ (see Fig. 3) is charged from $V_{cc}/3$ to $2V_{cc}/3$ in $(R_1 + R_2)C \ln(2)$ seconds. Considering that a first-order RC circuit is formed by R_1, R_2 and C, the voltage $V_c(t)$ which is developed across C and the current $I(t)$, drawn by the power

---

[2]All equations have been experimentally verified, with the experimental results deviating from the corresponding theoretical values by ± 5 μW.

TABLE I
EXAMPLE OF TWO TAGS WITH DIFFERENT DUTY CYCLE D

R_1(kΩ)	R_2(kΩ)	D(%)	P_{tot}(μW)	$P(a_1)$
3.95	8.6	60	989	$(1.81A^2)/\pi^2$
10.35	5.4	75	545	A^2/π^2

supply, are given by:

$$V_c(t) = V_{cc}(1 - e^{\frac{-t}{(R_1+R_2)C}}) + V_c(0)\, e^{\frac{-t}{(R_1+R_2)C}}, \quad (9)$$

$$I(t) = \frac{V_{cc} - V_c(t)}{R_1 + R_2}, \quad (10)$$

where $V_c(0) = V_{cc}/3$ is the initial condition of the capacitor voltage. Thus, using (9) and (10), the average power P_{ch} drawn by the power source, V_{cc}, during a period of $1/F$, is calculated as follows:

$$P_{ch} = F \int_0^{(R_1+R_2)C\ln(2)} V_{cc}\, I(t)\, dt \quad (11)$$

$$= \frac{V_{cc}^2}{3(R_1 + 2R_2)\ln(2)}. \quad (12)$$

As stated above, current flows through R_1 while timer output is "low", discharge pin is grounded (and the RF transistor is "on") and thus, the average power drawn by R_1 is given by:

$$P_{R_1} = \frac{(1-D)V_{cc}^2}{R_1} \quad (13)$$

$$\stackrel{(2)}{=} \frac{V_{cc}^2}{R_1^2/R_2 + 2R_1}. \quad (14)$$

Power consumed during discharge is the dominant power consumption factor. As an example, a typical tag with $R_1 = 5.3$ kΩ, $R_2 = 10.6$ kΩ and $C = 730$ pF operating at $F_{sw} = 74.5$ kHz consumes $P_{ch} = 92$ μW, $P_d = 77$ μW and $P_{R_1} = 385$ μW, resulting in $P_{tot} = 775$ μW. Such a low power consumption results in the minimization of the power-source capacity requirements, thus further reducing the installation cost of the proposed WSN. Increasing R_1 reduces P_{R_1} but such an approach would also degrade the communication performance, as described in the following paragraph.

The implemented receiver is dependent on the power of the *fundamental* subcarrier frequency of the backscattered signal, which is given by [36]:

$$P(a_1) = \left[\frac{A\sqrt{2}}{\pi}\sin(\pi D)\right]^2, \quad (15)$$

where D is the duty cycle and A is the peak-to-peak amplitude of the pulse signal. For $D = 50$ %, the value of $P(a_1)$ is maximized; when D is higher (or lower) than 50 %, the power of the fundamental frequency is decreased.

For example, considering the case of two tags with the same subcarrier frequency of 50 kHz, where one tag has $D = 60$ % and the other has $D = 75$ %, then the total power consumption and power of their fundamental frequencies are calculated using (1), (2) and (15). The corresponding results are presented in Table I. It is observed that the sensor/tag with $D = 60$ %
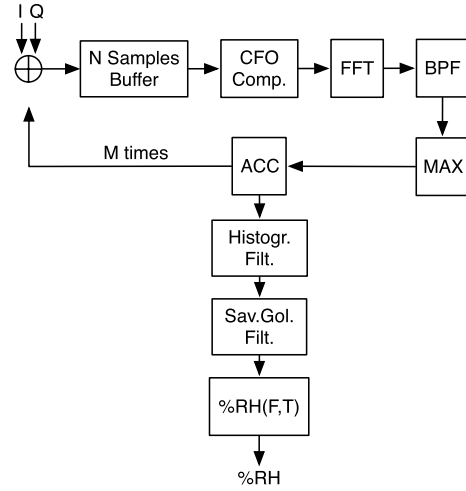

Fig. 11. Sensor's subcarrier frequency value is estimated using periodogram detection. After a set of data is collected, the aforementioned filtering is applied.

consumes approximately 2 times more power than the one with $D = 75$ %, but the latter lacks power in its fundamental frequency by a factor of 1.81, which in turn will result in less accurate reception, as explained in the following section.

III. SOFTWARE-DEFINED RECEIVER DESIGN

For the implementation of the receiver, a commodity software-defined homodyne radio platform has been utilized, connected to a host PC. As shown in Fig. 11, the received baseband in-phase (I) and quadrature (Q) digitized signal samples are processed using suitable software running in the host PC. The difference in carrier frequency between the reader and the emitter (i.e. Carrier Frequency Offset, CFO) results in a variance between the real value and the estimated values of the subcarrier signals. In order to compensate this frequency shift, the difference between the nominal carrier value and the estimated one is calculated after the samples are collected, and then, all samples are frequency-shifted accordingly.

Subsequently, the *periodogram* of the received signal is calculated and the fundamental subcarrier frequency of the i-th tag is calculated as follows [33]:

$$\hat{F}_i = \arg\max_{F \in [F_{Li}, F_{Hi}]} |X(F)|^2, \quad (16)$$

where $X(F)$ is the Fourier transform of the received signal and F_{Li}, F_{Hi} denote the lowest and highest possible frequency output of the i-th tag, respectively, which are a-priori known. Thus, the frequency component with the maximum power for each spectrum band is estimated as the corresponding sensor's output frequency.

In order to reduce the error introduced from the wireless channel and the thermal noise at the receiver, a two-phase filtering process is implemented. Specifically, all $\hat{F}_i$s are estimated over a period of 10 minutes and stored in an accumulator, thus, producing vector $\vec{\hat{F}}_i$. The first phase of the filtering process, considers that the changes of the environmental humidity during that time interval are negligible.
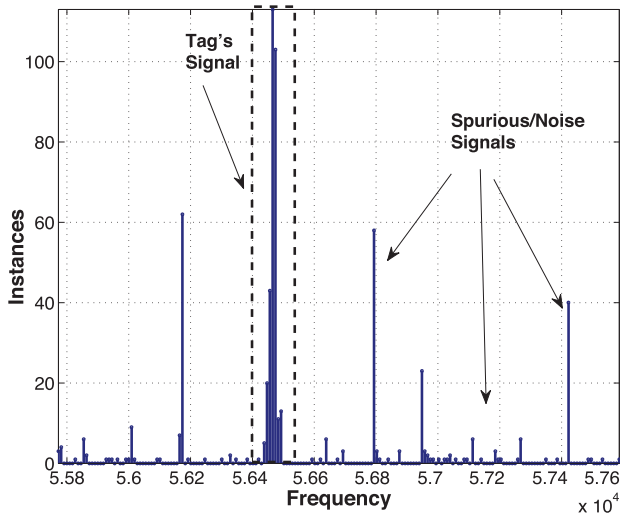
Fig. 12. Histogram filtering: A set of measurements is collected and their histogram is calculated. Only measurements within a certain range and with the highest occurrence are kept.

Then, a histogram with 200 frequency bins is calculated (corresponding to a frequency resolution of 10 Hz for a sensor's bandwidth of 2 kHz). The true value is located at the most prominent bins in the histogram (most frequent values), while the noisy outliers are less frequent. An example of such a histogram is depicted in Fig. 12. In order to take advantage of this fact, the F_is that belong to a certain range are kept intact and their mean value μ is calculated. The samples outside this range are set to $F_i = \mu$. The frequency range is determined by sliding a window of length $= N_B$ bins across the histogram and calculating the in-window sample cardinality. The window containing the bins, that correspond to the most frequent samples is used to calculate the frequency range that is utilized for the filtering.

The second phase utilizes a Savitzky-Golay filtering process [37], which is largely adopted in data smoothing applications [38]. This type of filtering exploits least-squares data smoothing on each subset of the measurement dataset. The critical parameters for this process are the order of the polynomial and the number of samples that the fitting operation is applied to. Thorough experimentation with real data demonstrated that the appropriate polynomial order and subset size are 3 and 201, respectively.

The two-phase process described above results in a significantly reduced error; in some cases, more than an order of magnitude reduction, in terms of the resulting mean error. The performance of each phase of the filtering process is illustrated in Fig. 13. Extensive real-dataset results before and after the filtering application are given in Section IV.

IV. NUMERICAL AND EXPERIMENTAL RESULTS

A. Communication Range and Accuracy Results

In order to investigate the performance of the proposed WSN in terms of sensing accuracy and maximum communication range, various experiments were conducted. A Silabs Si1004 development kit was utilized as a carrier emitter at

UHF (specifically at 868 MHz), with a transmission power of 20 mW (the maximum permissible limit, which is imposed by European directives is 3.2 W) and a commodity SDR reader (Ettus USRP N200) was utilized as the software-defined receiver. The carrier emitter, the receiver and a sensor/tag with subcarrier center frequency at 75 kHz were installed on poles of 1.7 m height. Communication performance was tested for various installation topologies by simultaneously comparing the estimated sensor's subcarrier frequency at the reader and the output frequency on the sensor/tag, using a frequency data-logger. The corresponding results are presented in Table II, where each row contains the emitter-to-tag distance (d_{et}), tag-to-reader distance (d_{tr}), the receiving window duration per measurement, and the resulting accuracy results in terms of various metrics, before and after the two-step filtering process.

The metrics employed to evaluate the accuracy performance of the proposed WSN are the mean square error (MSE), the root mean squared error (RMSE) and the mean relative error (MRE). The relative error is calculated by dividing the mean absolute error in Hz with the bandwidth of the tag (in this case 2 kHz) and multiplying the result by 100, thus, providing an estimate of the corresponding relative humidity (%RH) error.

For each experiment, both pre-filtering and post-filtering results are reported. It is observed that for the highlighted experiments 6, 10, 13, 18, the MRE is greatly reduced (by one order of magnitude in most cases). For example, in the case of experiment 13, the MRE of 14.72 % indicates that the sensor in this particular setup would be unusable without data filtering. However, after the specific filtering was applied, the MRE was reduced to 3.54 %, offering sensor results in that topology which are useable for the target environmental monitoring application. Therefore, the proposed filtering process, effectively yields higher signal-to-noise ratio (SNR) and longer communication distances.

Nevertheless, the designed filter is not indispensable in high-SNR communication links. For example, filtering in experiments 5 and 20 of Table II apparently increased the measurement error. That was due to the fact that in the particular high-SNR experiments, only a small number of frequency estimations were erroneous and the filtering process treated more samples than needed as erroneous. However, the error increase was still too small (on the order of 0.1 %) to be important, due to the high received SNR.

Finally, it is remarked that end-to-end measurement accuracy depends on both the sensing error (related to the sensing capacitor and conversion from capacitance to frequency through the 555 timer), as well as the reception error (related to the noise and sensitivity of the SDR reader). The first type of error was discussed in Figs. 9 and 10 of Section II.C, while the second type of error is described through Table II above. For example, case 8 of Table II offers an RMSE of 4 Hz (after filtering) in measuring subcarrier frequency at the SDR receiver (due to receiver noise), for a sensor bandwidth of 2 kHz. That corresponds to $100 \cdot 4/2000 = 0.2$ %RH RMS error. However, sensing and conversion of capacitance-to-frequency offers an RMS error of 2.5 %RH (as discussed in II.C). Thus, in this particular scenario, the end-to-end RMS error is dominated by the
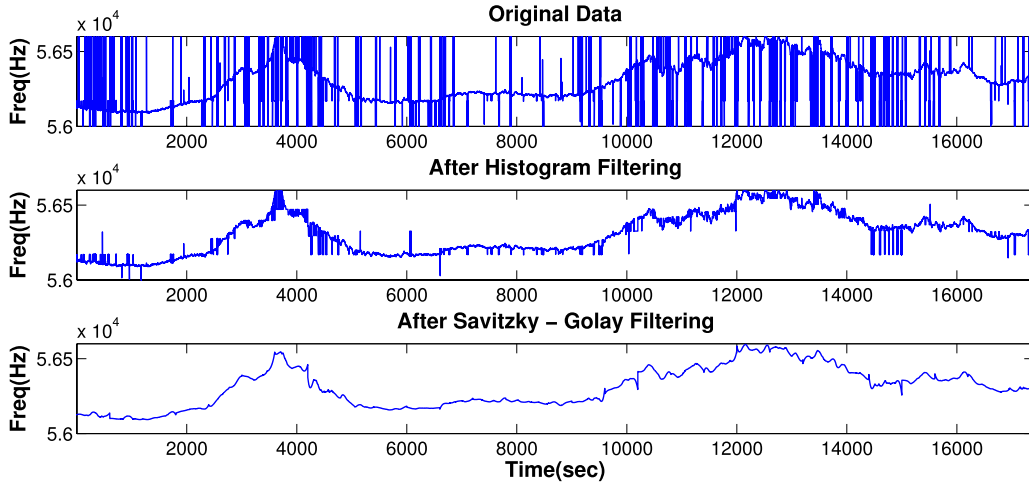
Fig. 13. Filtering process of received measurements. Histogram filtering followed by Savitzky-Golay filtering is applied.

TABLE II

COMMUNICATION DISTANCES AND ACCURACY

#	d_{et}(m)	d_{tr}(m)	Sampling Window(ms)	MSE(Hz^2) pre-filt.	MSE(Hz^2) post-filt.	RMSE(Hz) pre-filt.	RMSE(Hz) post-filt.	MRE(%) pre-filt.	MRE(%) post-filt.
1	2	134	1000	54.46	9.75	7.38	3.12	0.14	0.12
2	2	134	100	17.16	15.50	4.14	3.94	0.11	0.15
3	2	134	10	152.16	72.60	12.34	8.52	0.51	0.28
4	8	128	1000	76.16	49.95	8.73	7.07	0.16	0.22
5	8	128	100	10.24	135.18	3.20	11.63	0.10	0.34
6	**8**	**128**	**10**	**193900.97**	**716.90**	**440.34**	**26.78**	**12.04**	**1.05**
7	16	120	1000	88.72	22.86	9.42	4.78	0.16	0.19
8	16	120	100	731.74	16.40	27.05	4.05	0.19	0.17
9	16	120	50	41056.04	911.64	202.62	30.19	2.52	1.33
10	**16**	**120**	**25**	**171627.62**	**1273.66**	**414.28**	**35.69**	**9.85**	**1.54**
11	24	112	1000	5401.59	56.69	73.50	7.53	0.53	0.31
12	24	112	100	113869.83	2341.03	337.45	48.38	6.72	2.02
13	**24**	**112**	**50**	**249770.93**	**6151.26**	**499.77**	**78.43**	**14.72**	**3.54**
14	32	104	1000	281290.67	16040.71	530.37	126.65	12.36	5.02
15	32	104	100	437375.95	63415.15	661.34	251.82	22.01	12.45
16	52	84	1000	1996.34	24.96	44.68	5.00	0.22	0.20
17	52	84	100	4753.10	30.66	68.94	5.54	0.34	0.22
18	**86**	**50**	**1000**	**3510.00**	**65.09**	**59.25**	**8.07**	**8.13**	**3.14**
19	86	50	100	6526.23	47.02	80.79	6.86	0.55	0.30
20	96	40	1000	10.32	17.28	3.21	4.16	0.1	0.19
21	96	40	100	20.68	13.44	4.55	3.67	0.08	0.15
22	96	40	25	177744.15	2484.94	421.60	49.85	7.37	2.25

sensing error. For other cases of Table II, the end-to-end RMS error can be calculated exploiting independence of the two errors, as follows:

$$\text{RMSE} = \sqrt{\text{RMSE}_1^2 + \text{RMSE}_2^2}, \qquad (17)$$

where RMSE_1, RMSE_2 is the RMS value of the sensing and the reception error, respectively.

B. Experimental WSN in a Greenhouse

Environmental humidity is a *critical* parameter in greenhouse monitoring, since high relative humidity on plant surfaces promotes the growth of various disease organisms (such as *Botrytis cinerea*) [24]. Moreover, under saturated humidity conditions plant's evaporation mechanism deteriorates, resulting in decreased nutrient absorption [25]. In order

to evaluate the performance of the proposed environmental monitoring system in a real-world scenario, a sensor network with the aforementioned analog scatter-radio principles was implemented and deployed in a tomato greenhouse at the Mediterranean Agronomic Institute of Chania (MAICh, www.maich.gr).

The WSN consists of 10 environmental relative humidity sensors. In order to increase communication coverage, two carrier emitters with a transmitting power of 20 mW each, illuminate the sensors with carrier waves alternatively in time (TDMA). The network topology is depicted in Fig. 14-left, where the locations of the sensors, the emitters, the software-defined receiver and the host laptop computer are indicated. All tags/sensors and emitters where placed in IP65-rated enclosures hanging from the ceiling (Fig. 14-right). All sensors were fabricated with different RC components, based on (5) and (6) in order to implement the FDMA
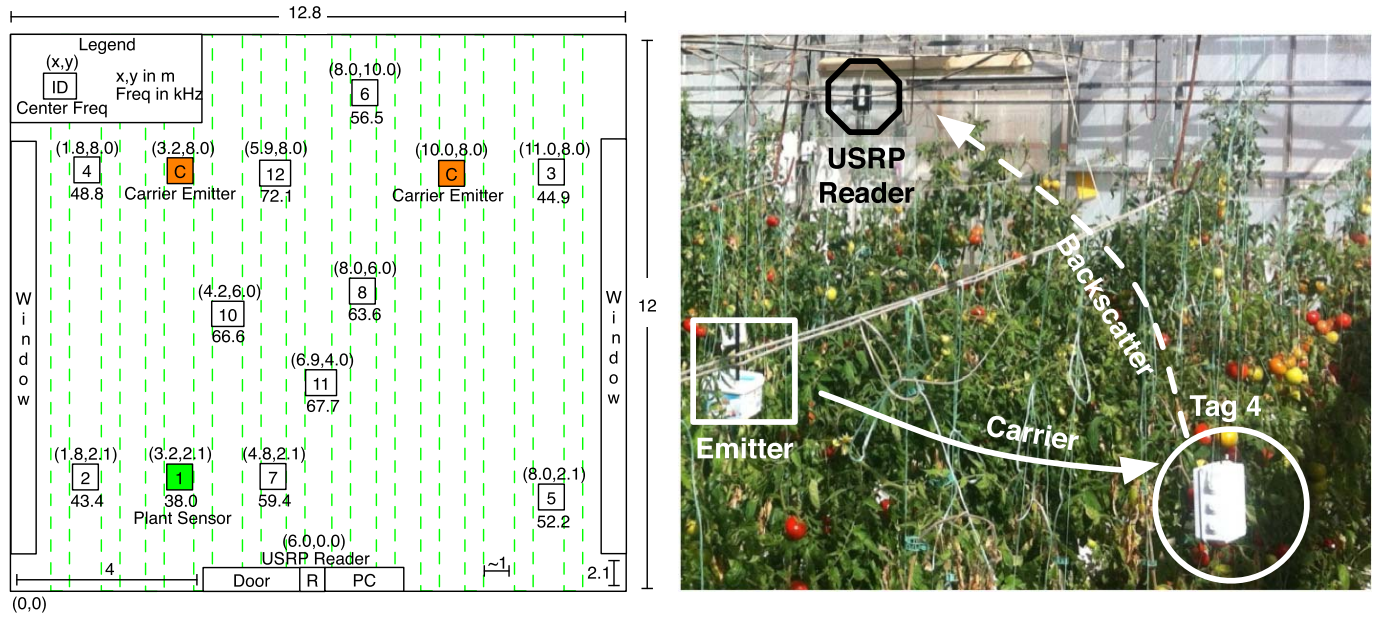
Fig. 14. Left: Experimental network topology. 10 %RH sensors, 1 plant voltage sensor and 2 carrier emitters with transmit power at 20 mW were deployed. Right: Photo of the deployment inside the greenhouse.
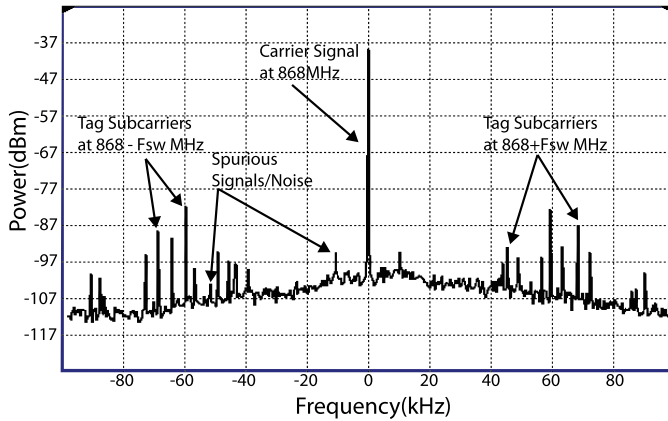

Fig. 15. Periodogram from multiple sensors in the greenhouse. Each tag operates in a distinct frequency band.
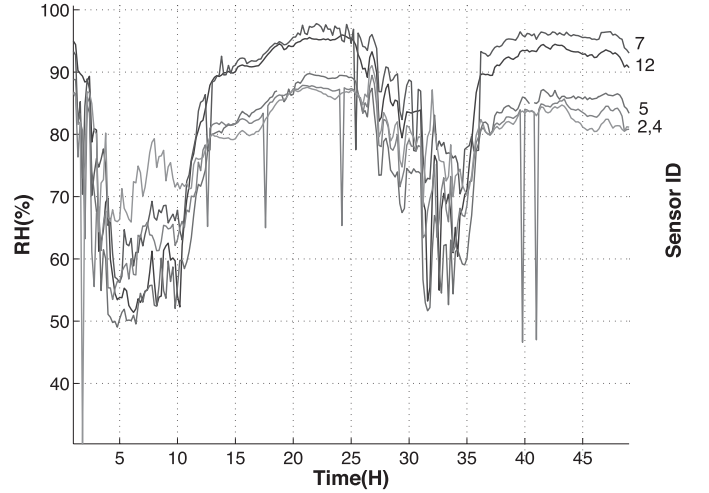

Fig. 16. Data collected from multiple tags inside the tomato greenhouse for a total of 48 hours. Differences in %RH are due to the variability of microclimatic conditions across the greenhouse (e.g. tags closer to the window exhibit smaller %RH values).

scheme described in Section II. The network's periodogram is depicted in Fig. 15, where the subcarriers of the individual tags can be observed. The spurious signals are filtered out in the software-defined receiver via the process described in Section III.

The processing of the received backscatter signals was conducted using a low-cost laptop hosting the software-defined receiver. The estimated relative humidity values were uploaded at a remote web database. The data that were collected during more than 48 hours of monitoring are depicted in Fig. 16. Although the sensors exhibit similar behavior, differences in the humidity values, which were recorded by the individual sensors, are also observed. This is due to the different microclimatic environmental conditions which prevail at the installation location of each sensor. For example sensors which are closer to windows measure lower humidity values than ones that are placed closer to the center of the greenhouse, especially during the night.

C. Comparison With Classic WSNs

Duty cycling (i.e. periodically transmitting and then falling to idle-mode) is utilized by classic radio WSN nodes in order to decrease the energy consumption per measurement, thus extending WSN lifetime. In this work, the sensor tags are designed such that they consume low power; utilization of duty cycling could further decrease the required energy requirements per measurement. Experimentation with various receiving window durations provided an indication about the smallest time period that the sensors should remain in the 'active' state in order to scatter the acquired measurement with an acceptable error. However, there is an inherent communication tradeoff: by decreasing duration of the receiving window

TABLE III

COMPARISON OF ENERGY CONSUMPTION PER MEASUREMENT IN THE
PROPOSED AND CLASSIC WSN RADIO MODULES

Comm. Module	Bit-rate (kbps)	Power (mW)	Time "on" (ms)	Energy (mJ/measurement)
CC2500	2.4	42.4	26.7	1.132
CC2500	10	42.4	6.4	0.271
CC2500	100	42.4	0.64	0.03
CC2500	250	42.4	0.256	0.01
This Work	–	0.72	1000	0.72
This Work	–	0.72	100	0.072
This Work	–	0.72	50	0.036
This Work	–	0.72	10	0.007

(and thus, the number of received signal samples at the receiver), signal-to-noise ratio will also be decreased. Therefore, smaller receiving window durations result in degraded communication performance. As demonstrated in Table II, the receiving window duration (i.e. sampling window) can be as small as 10 ms for relatively small d_{et} distances (experiment 3) and down to 100 ms for longer distances (experiments 8, 12, 17, 19, 21). On the other hand, the sampling window of 1 sec outperforms narrower sampling windows.

The energy consumption per measurement transmission for a classic WSN module, typically consisting of a microcontroller and an active, low-power ZigBee-type radio, is given by:

$$E_{wsn} = \frac{N_b}{F_{tx}} P_{tx}, \qquad (18)$$

where N_b is the number of bits per measurement transmission, F_{tx} is the data rate (in bits per second) and P_{tx} is the power consumption (in Watts). On the other hand, the energy per measurement for the developed analog humidity sensor with scatter-radio is given by:

$$E_{bs} = T_{bs} \ P_{bs}, \qquad (19)$$

where T_{bs} is the receiving window duration (in sec) needed for reliable backscattering of humidity measurement and P_{bs} is the power consumption of the sensor (in Watts). A comparison (in Joules per measurement) between the two approaches is given in Table III. For the classic WSN radio, a packet of 64 bits per measurement was assumed, transmitted at 0 dBm power (as for example in a state-of-the-art low-power WSN radio module). In particular, for the case of a 100 ms receiving window, the analog scatter-radio sensor outperforms the active radio for data rates smaller than 100 kbps. Moreover, for receiving windows of 10 ms, the proposed sensor outperforms the classic WSN radio module, regardless bit-rate. It is important to note that for particular applications such as %RH monitoring inside a greenhouse, accuracy of measurement is not a major issue and even an MRE of 5 % is tolerable. Therefore, smaller sampling windows can be utilized safely, regardless of the measurement accuracy degradation, which, however, remains at an acceptable level (e.g. MRE 1.05 % for 10 ms).

These results demonstrate the potential of the proposed WSN to achieve reliable transmission of collected measurements, with low cost and low power consumption for short-range environmental monitoring applications on the order of 100 m range.

V. CONCLUSION

This paper presented the development of a novel WSN for environmental relative humidity monitoring, using *analog* scatter-radio-enabled sensors that consume less than 1 mW of power and offer communication range above 100 m. The proposed WSN utilized frequency division multiple access that allowed all receiver-less sensors to communicate in a collision-free manner and is ideal for low-bitrate environmental monitoring. The multipoint surface fitting calibration, in conjunction with the two-phase filtering process, provided a mean absolute error of 1.9 %RH for a temperature range of 10–50 °C. Additionally, it was demonstrated that the energy consumption per measurement of the proposed WSNs is lower than that of a ZigBee-type WSN. The proposed WSN is suitable for distributed monitoring of environmental parameters in large-scale, precision agriculture applications. Future work will focus on further deceasing the power consumption of the proposed joint sensor-scatter radio communicator design, by at least one order of magnitude.

REFERENCES

[1] A. Thakkar and K. Kotecha, "Cluster head election for energy and delay constraint applications of wireless sensor network," *IEEE Sensors J.*, vol. 14, no. 8, pp. 2658–2664, Aug. 2014.

[2] W. Y. Toh, Y. K. Tan, W. S. Koh, and L. Siek, "Autonomous wearable sensor nodes with flexible energy harvesting," *IEEE Sensors J.*, vol. 14, no. 7, pp. 2299–2306, Jul. 2014.

[3] S. Mini, S. K. Udgata, and S. L. Sabat, "Sensor deployment and scheduling for target coverage problem in wireless sensor networks," *IEEE Sensors J.*, vol. 14, no. 3, pp. 636–644, Mar. 2014.

[4] R. Yao, W. Wang, M. Farrokh-Baroughi, H. Wang, and Y. Qian, "Quality-driven energy-neutralized power and relay selection for smart grid wireless multimedia sensor based IoTs," *IEEE Sensors J*, vol. 13, no. 10, pp. 3637–3644, Oct. 2013.

[5] G. Tolle *et al.*, "A macroscope in the redwoods," in *Proc. ACM Embedded Netw. Sensor Syst. (SenSys)*, San Diego, CA, USA, Nov. 2005, pp. 51–63.

[6] G. Tan and A.-M. Kermarrec, "Greedy geographic routing in large-scale sensor networks: A minimum network decomposition approach," *IEEE/ACM Trans. Netw.*, vol. 20, no. 3, pp. 864–877, Jun. 2012.

[7] S. Zhang, G. Tan, H. Jiang, B. Li, and C. Wang, "On the utility of concave nodes in geometric processing of large-scale sensor networks," *IEEE Trans. Wireless Commun.*, vol. 13, no. 1, pp. 132–143, Jan. 2014.

[8] J. Lee and C. Tepedelenlioglu, "Distributed detection in coexisting large-scale sensor networks," *IEEE Sensors J.*, vol. 14, no. 4, pp. 1028–1034, Apr. 2014.

[9] D. Arifler, "Optimality of homogeneous sensing range assignment in large-scale wireless sensor network deployments," *IEEE Commun. Lett.*, vol. 16, no. 9, pp. 1489–1491, Sep. 2012.

[10] G. Shi, J. Zheng, J. Yang, and Z. Zhao, "Double-blind data discovery using double cross for large-scale wireless sensor networks with mobile sinks," *IEEE Trans. Veh. Technol.*, vol. 61, no. 5, pp. 2294–2304, Jun. 2012.

[11] Y. Liu *et al.*, "Does wireless sensor network scale? A measurement study on GreenOrbs," in *Proc. IEEE Int. Conf. Comput. Commun. (INFOCOM)*, Shanghai, China, Apr. 2011, pp. 873–881.

[12] L. Mottola and G. P. Picco, "Programming wireless sensor networks: Fundamental concepts and state of the art," *ACM Comput. Surv.*, vol. 43, no. 3, pp. 19:1–19:51, Apr. 2011.

[13] H. Stockman, "Communication by means of reflected power," *Proc. IRE*, vol. 36, no. 10, pp. 1196–1204, Oct. 1948.

[14] S. Thomas and M. S. Reynolds, "QAM backscatter for passive UHF RFID tags," in *Proc. IEEE RFID Conf.*, Orlando, FL, USA, Apr. 2010, pp. 210–214.

[15] Y. Ling *et al.*, "A printable CNT-based FM passive wireless sensor tag on a flexible substrate with enhanced sensitivity," *IEEE Sensors J.*, vol. 14, no. 4, pp. 1193–1197, Apr. 2014.

[16] D. M. Dobkin, *The RF in RFID: Passive UHF RFID in Practice*. Amsterdam, The Netherlands: Elsevier, 2008.

[17] J. Kimionis, A. Bletsas, and J. N. Sahalos, "Bistatic backscatter radio for tag read-range extension," in *Proc. IEEE Int. Conf. RFID-Technol. Appl. (RFID-TA)*, Nice, France, Nov. 2012, pp. 356–361.

[18] G. Vannucci, A. Bletsas, and D. Leigh, "A software-defined radio system for backscatter sensor networks," *IEEE Trans. Wireless Commun.*, vol. 7, no. 6, pp. 2170–2179, Jun. 2008.

[19] J. Kimionis, A. Bletsas, and J. N. Sahalos, "Increased range bistatic scatter radio," *IEEE Trans. Commun.*, vol. 62, no. 3, pp. 1091–1104, Mar. 2014.

[20] V. Lakafosis, A. Rida, R. Vyas, L. Yang, S. Nikolaou, and M. M. Tentzeris, "Progress towards the first wireless sensor networks consisting of inkjet-printed, paper-based RFID-enabled sensor tags," *Proc. IEEE*, vol. 98, no. 9, pp. 1601–1609, Sep. 2010.

[21] A. P. Sample, D. J. Yeager, P. S. Powledge, and J. R. Smith, "Design of a passively-powered, programmable sensing platform for UHF RFID systems," in *Proc. IEEE RFID Conf.*, Grapevine, TX, USA, Mar. 2007, pp. 149–156.

[22] E. Kampianakis, S. D. Assimonis, and A. Bletsas, "Network demonstration of low-cost and ultra-low-power environmental sensing with analog backscatter," in *Proc. IEEE Topical Meeting Wireless Sensors Sensor Netw. (WiSNet)*, Newport Beach, CA, USA, Jan. 2014, pp. 61–63.

[23] E. Kampianakis, J. Kimionis, K. Tountas, and A. Bletsas, "A remotely programmable modular testbed for backscatter sensor network research," in *Proc. 5th Workshop Real-World Wireless Sensor Netw. (REALWSN)*, Como Lake, Italy, Sep. 2013, pp. 153–161.

[24] M. A. Eden, R. A. Hill, R. Beresford, and A. Steward, "The influence of inoculum concentration, relative humidity, and temperature on infection of greenhouse tomatoes by *botrytis cinerea*." *Plant Pathol.*, vol. 45, no. 4, pp. 795–806, Aug. 1996.

[25] L. Mortensen, "Effect of relative humidity on growth and flowering of some greenhouse plants," *Sci. Horticulturae*, vol. 29, no. 4, pp. 301–307, Aug. 1986.

[26] K. Lasanen and J. Kostamovaara, "A 1.2-V CMOS *RC* oscillator for capacitive and resistive sensor applications," *IEEE Trans. Instrum. Meas.*, vol. 57, no. 12, pp. 2792–2800, Dec. 2008.

[27] Z. Tan, R. Daamen, A. Humbert, Y. V. Ponomarev, Y. Chae, and M. Pertijs, "A 1.2-V 8.3-nJ CMOS humidity sensor for RFID applications," *IEEE J. Solid-State Circuits*, vol. 48, no. 10, pp. 2469–2477, Oct. 2013.

[28] A. D. DeHennis and K. D. Wise, "A wireless microsystem for the remote sensing of pressure, temperature, and relative humidity," *J. Microelectromech. Syst.*, vol. 14, no. 1, pp. 12–22, Feb. 2005.

[29] D. Cirmirakis, A. Demosthenous, N. Saeidi, and N. Donaldson, "Humidity-to-frequency sensor in CMOS technology with wireless readout," *IEEE Sensors J.*, vol. 13, no. 3, pp. 900–908, Mar. 2013.

[30] C. Alippi, R. Camplani, C. Galperti, and M. Roveri, "A robust, adaptive, solar-powered WSN framework for aquatic environmental monitoring," *IEEE Sensors J.*, vol. 11, no. 1, pp. 45–55, Jan. 2011.

[31] H.-C. Lin, Y.-C. Kan, and Y.-M. Hong, "The comprehensive gateway model for diverse environmental monitoring upon wireless sensor network," *IEEE Sensors J.*, vol. 11, no. 5, pp. 1293–1303, May 2011.

[32] T. W. Davis, X. Liang, C.-M. Kuo, and Y. Liang, "Analysis of power characteristics for sap flow, soil moisture, and soil water potential sensors in wireless sensor networking systems," *IEEE Sensors J.*, vol. 12, no. 6, pp. 1933–1945, Jun. 2012.

[33] E. Kampianakis, "Scatter radio sensor network with analog frequency modulation principles," M.S. thesis, Dept. Electron. Comput. Eng., Tech. Univ. Crete, Chania, Greece, 2014.

[34] A. Bletsas, S. Siachalou, and J. N. Sahalos, "Anti-collision backscatter sensor networks," *IEEE Trans. Wireless Commun.*, vol. 8, no. 10, pp. 5018–5029, Oct. 2009.

[35] S. Haykin, *Communication Systems*. New York, NY, USA: Wiley, 2009.

[36] S. W. Smith, *The Scientist and Engineer'S Guide to Digital Signal Processing*. San Diego, CA, USA: California Technical Publishing, 1997.

[37] R. W. Schafer, "What is a Savitzky-Golay filter? [Lecture Notes]," *IEEE Signal Process. Mag.*, vol. 28, no. 4, pp. 111–117, Jul. 2011.

[38] K. Pandia, S. Ravindran, R. Cole, G. Kovacs, and L. Giovangrandi, "Motion artifact cancellation to obtain heart sounds from a single chest-worn accelerometer," in *Proc. IEEE Int. Conf. Acoust., Speech, Signal Process. (ICASSP)*, Dallas, TX, USA, Mar. 2010, pp. 590–593.

Eleftherios Kampianakis (S'13) received the Engineering Diploma in electronic and computer engineering from the Technical University of Crete, Chania, Greece, in 2011, where he is currently pursuing the M.Sc. degree, and is a Graduate Researcher with the Telecom Laboratory. As an Undergraduate Researcher, he developed over the air programmed WSN testbeds with low-power software-defined radio transceivers while his work as a Graduate Researcher regards low-power, low-cost, and large-scale scatter radio WSN. In particular, he focuses on scatter radio networking, low-power scatter radio front-end design, software-defined radio, and low-power environmental sensing.

He has received a fellowship award for his graduate studies, and was also a recipient of the Best Diploma Thesis Award on the IEEE Vehicular Technology Society and Aerospace and Electronic Systems Society's Joint Greece Chapter Final/Diploma Thesis Competition.

John Kimionis (S'10) received the Engineering Diploma and M.Sc. degree in electronic and computer engineering from the Technical University of Crete, Chania, Greece, in 2011 and 2013, respectively, where he was an Undergraduate/Graduate Researcher with the Telecom Laboratory, involved in backscatter radio communication for large-scale and low-cost wireless sensor networks. He is currently pursuing the Ph.D. degree at the School of Electrical and Computer Engineering, Georgia Institute of Technology, Atlanta, GA, USA. He is currently a member of the ATHENA Research Group, where he is involved in microwave and RF engineering, and rapid electronics prototyping. His main focus was in the areas of backscatter radio and RFID, wireless sensor networks, software-defined radio for backscatter radio and sensor networks, and telecom modules/communication algorithms development.

His main research interests are the design of low-cost RF front-ends for backscatter radio tags/sensors and fabrication techniques with inkjet printing. Coupling these with his communication background, he aims on significantly extending the range of backscatter radio sensors, while maintaining low-power consumption of the tags.

Mr. Kimionis has received fellowship awards for his undergraduate and graduate studies, and was a recipient of the Second Best Student Paper Award at the IEEE International Conference on RFID-Technologies and Applications, Barcelona, Spain, in 2011.

Konstantinos Tountas is currently pursuing the Degree at the School of Electronic and Computer Engineering, Technical University of Crete, Chania, Greece. His research interests focus on wireless communications and networking, radio hardware/software implementations for wireless transceivers, and low-cost backscatter sensor networks and RFID.

Christos Konstantopoulos was born in Athens, Greece, in 1989. He received the B.Sc. degree from the School of Electronic and Computer Engineering, Technical University of Crete, Chania, Greece, in 2012, where he is currently pursuing the M.Sc. degree. As an undergraduate student, he developed a power management system for the maximization of the energy that comes from flexible photovoltaic cells. Currently, as a Graduate Researcher, he is involved in a microelectronic system for ultralow-energy harvesting that is applicable to low-power backscatter networks.

His research interests include power electronics for Renewable Energy Sources (RES), energy harvesting for wireless sensor networks, and electronic measurement systems.

Eftichios Koutroulis (M'10) was born in Chania, Greece, in 1973. He received the B.Sc. and M.Sc. degrees and the Ph.D. degree in power electronics and Renewable Energy Sources (RES) from the School of Electronic and Computer Engineering, Technical University of Crete, Chania, in 1996, 1999, and 2002, respectively, where he is currently an Assistant Professor. His research interests include power electronics (dc/ac inverters and dc/dc converters), the development of microelectronic energy management systems for RES, and the design of photovoltaic and wind energy conversion systems.

Aggelos Bletsas (S'03–M'05–SM'14) received the Diploma (Hons.) degree in electrical and computer engineering from the Aristotle University of Thessaloniki, Thessaloniki, Greece, in 1998, and the S.M. and Ph.D. degrees from the Massachusetts Institute of Technology, Cambridge, MA, USA, in 2001 and 2005, respectively. He was with Mitsubishi Electric Research Laboratories, Cambridge, as a Post-Doctoral Fellow, and with the Radiocommunications Laboratory, Department of Physics, Aristotle University of Thessaloniki, as a Visiting Scientist. He joined the School of Electronic and Computer Engineering, Technical University of Crete, Chania, Greece, in Summer 2009, as an Assistant Professor, and promoted to Associate Professor in 2014.

His research interests span the broad area of scalable wireless communication and networking, with emphasis on relay techniques, backscatter communications and RFID, energy harvesting, radio hardware/software implementations for wireless transceivers, and low-cost sensor networks. His current vision and focus is on single-transistor front-ends and backscatter sensor networks, for large-scale environmental sensing. He is the Principal Investigator of the project BLASE: Backscatter Sensor Networks for Large-Scale Environmental Sensing, funded by the General Secretariat of Research and Technology Action Proposals evaluated positively from the 3rd European Research Council Call. He is also a Management Committee Member and National Representative in the European Union COST Action IC1301 Wireless Power Transmission for Sustainable Electronics. He is an Associate Editor of the IEEE WIRELESS COMMUNICATIONS LETTERS since its foundation and a Technical Program Committee Member of flagship IEEE conferences. He holds two patents from USPTO.

Dr. Bletsas was a co-recipient of the IEEE Communications Society's Marconi Prize Paper Award in Wireless Communications in 2008, the Best Paper Distinction at the International Symposium on Wireless Communication Systems, Siena, Italy, in 2009, and the Second Best Student Paper Award at the IEEE International Conference on RFID-Technologies and Applications, Barcelona, Spain, in 2011. Two of his undergraduate advisees were winners of the 2009–2011 and 2011–2012 Best Diploma Thesis contest, respectively, among all Greek Universities on Advanced Wireless Systems, awarded by the IEEE VTS/AES joint Greek Chapter. He was also a recipient of the Technical University of Crete 2013 Research Excellence Award in 2013.